Aalborg Universitet

Containment-based Distributed Coordination Control to Achieve Both Bounded Voltage and Precise Current Sharing in Reverse-Droop-based DC Microgrid

Renke Han[1*], Haojie Wang[2], Zheming Jin[1], Lexuan Meng[1], Josep M. Guerrero[1]

[1] Department of Energy Technology, Aalborg University, Aalborg, Denmark
[2] School of Electric and Electronic Engineering, North China Electric Power University, Beijing, China
* rha@et.aau.dk

Abstract—A highly flexible and reliable control strategy is proposed to achieve bounded voltage and precise current sharing, which is implemented in a reverse-droop-based dc Micro-Grid. To acquire the fast-dynamic response, the reverse droop control is used to replace the *V-I* droop control in the primary level. In the secondary level, the containment-based controller is proposed to bound the bus voltages within a reasonable range and keep the necessary voltage deviations for power flow regulation; the consensus-based controller is simultaneous involved to regulate power flow achieving accurate current sharing among converters. Combined the proposed controllers with the electrical part of the dc Micro-Grid, a model is fully developed to analyze the sensitivity of different control coefficients. Experimental results are presented to demonstrate the effectiveness of the proposed method.

Keywords—Containment-based distributed control, bounded voltage, current sharing, large signal model, dc microgrid

I. INTRODUCTION

With the increasing penetration of renewable energy sources into modern electric grid, the concept of Microgrid (MG) is identified as an effective method for power generation and distribution [1] [2]. The DC nature of emerging renewable energy sources efficiently lends itself to a dc MG paradigm [3]. In a decentralized control method, the conception of droop control is widely adopted to achieve communication-less current sharing among converters by imposing virtual resistances. Existing droop control can be classified into two groups: reverse droop (*I-V*) [4] and voltage droop (*V-I*) [5]. Compared with the voltage droop control, the dynamic response of reverse droop control is faster due to its single current control loop. However, no matter which droop control is implemented, voltage deviations from nominal value and current sharing errors still exist due to effects of virtual resistances and different line impedances. Considering the *V-I* droop as the primary control in the hierarchical control structure [6], the centralized secondary controller is proposed to achieve voltage restoration and improve current sharing in dc MG. But, the centralized controller suffers from high computational and low flexibility, while distributed control algorithm has emerged as an attractive alternative and offers improved reliability and simpler communication network. In [7], a decentralized controller is proposed to achieve the per unit load sharing through low-bandwidth communication. Meanwhile, an improved droop control in [8] by using average voltage and current values is proposed to improve the current sharing and restore the dc bus voltage. For the methods mentioned above, the broadcast communication is used to collect all the information from all the other DGs. To decrease the communication traffic, a voltage observer [9] is proposed to estimate the average voltage which is used to generate a voltage correction term to adjust the voltage reference, meanwhile the current regulator provides a resistance correction term based on the consensus-based communication [10]. Furthermore, a noise-resilient voltage observer combined with consensus-based voltage/current regulator is proposed to achieve more resilient control in dc MGs [11]. From the perspective of power flow in a dc MG, the terminal voltage from each converter is allowed to exist the deviation around the nominal value, otherwise there is no power flow between the nodes [12]. However, too large voltage deviations can cause stability problems and destroy power quality in the system. Accordingly, most of the existing literature are devoted to fix the average voltage at the nominal value rather than bounding the bus voltages within a reasonable range.

Considering above problems, a containment-based distributed controller is proposed to bound bus voltages within a reasonable range and keep the voltage deviations for power flow regulation. Then, the consensus-based current controller is involved to regulate the power flow achieving current sharing accurately. In addition, both the proposed methods are implemented based on a reverse droop controller for dc/dc converters to acquire the fast-dynamic response. Combining the proposed method with the electrical topology of dc MG, the model is established to analyse the sensitivity of different control coefficients. Finally, experimental results are shown to prove the effectiveness of the proposed method.

II. CONTAINMENT-BASED DISTRIBUTED COORDINATION CONTROL IN REVERSE DROOP BASED DC MG

This section explains proposed controllers based on the hierarchical control structure for a dc MG. The reverse droop control is explained in the primary control level. Furthermore, the proposed containment-based voltage controller and consensus-based current control is explained in detail in the secondary control level.

A. Definitions and Notations

For the control system with *n* distributed controllers, a controller is called a *leader* if it only provides information to

Fig. 1. Configuration of the Containment and Consensus-based Distributed Coordination Controller in a dc MG.

its neighbors and does not receive any information. A controller is called a *follower* if it can receive information from one or more neighbors through communication topology. Let N_i denote the set of i_{th}-controller neighbors chosen from followers, and R_i denote the set of leaders which can give its information to i_{th}-agent directly. This definition is applied to containment-based voltage controller, in which the dynamic range is appointed in charge of setting the lower and upper voltage boundaries respectively. Meanwhile, the consensus-based reactive power controller only uses the neighbors' information without the reference leaders' information.

Let C be a set in a real vector space $V \subseteq R^p$. The set C is called convex if, for any x and y in C, the point *(1-z)x+zy* is in C for any $z \in [0,1]$. The convex hull for a set of points $X=\{x_1,...,x_q\}$ in V is the minimal convex set containing all points in X. Let $Co(X)$ denote the convex hull of X. In particular, because of $V \subseteq R$, $Co(X)=\{x|x \in [min\ x_i,\ max\ x_i]\}$ which is used in this paper. In addition, define *n*-vector $Z \in R^n$, then $diag(Z) \in R^{n \times n}$ is defined as the diagonal matrix whose diagonal elements are the elements in vector *Z*. I_n is the unit matrix and $0_{[n]}$ is the zero $n \times n$ matrix. 0_n and 1_n are the *n*-vectors with all *0* and *1* elements.

Furthermore, for consensus-based current control, an adjacency matrix is defined as $A=[a_{ij}] \in R^{n \times n}$ with $a_{ij}>0$ if node *i* can receive information from node *j* otherwise $a_{ij}=0$; The Laplacian matrix is defined as $L_I = \left[l_{ij} \right] \in R^{n \times n}$ with $l_{ii} = \sum_{j=1}^{n} a_{ij}$ and $l_{ij} = -a_{ij}, i \neq j$. For containment-based control, another adjacency matrix is defined as $B = \left[b_{ij} \right] \in R^{n \times 2}$ with $b_{il}=1$ if node *i* can receive information from one of the two reference leaders otherwise $b_{il}=0$, in which *l* represents the label of two reference leaders; Another matrix is defined as $L_V' = \left[l_{ij} \right] \in R^{n \times (n+2)}$ with $l_{ii} = \sum_{j=1}^{n} a_{ij} + \sum_{l=n+1}^{n+2} b_{il}$; for other items, when *j<n*, $l_{ij}=-a_{ij}$, otherwise when *j>n*, $l_{ij}=-b_{ij}$. For

convenience, the matrix L_V' is divided into $L_V' = \begin{bmatrix} L_V & L_{Bou} \end{bmatrix}$ in which $L_V \in R^{n \times n}$ and $L_{Bou} \in R^{n \times 2}$.

B. Reverse Droop Control in the Primary Level

To acquire fast-dynamic response, the single current *PI* control loop is used to replace the voltage and current double control loop. Thus, the reverse droop controller is proposed to replace the outer voltage control loop, which is shown as

$$I_{refi} = \frac{V_{ref} - V_{ci}}{R_{viri}} \qquad (1)$$

where I_{refi} is the current reference for current *PI* controller, R_{viri} is the virtual resistance, V_{ci} is the bus voltage measured from the output capacitor.

In a dc MG, because the different line impedances connecting these DGs make the bus voltages from DGs as localized information, the output currents from DGs cannot be shared proportionally only by reverse droop control. Meanwhile, the reverse droop can also cause voltage deviations from the nominal value. Thus, the controller in the secondary control level should be proposed to achieve the precise current sharing and bound the bus voltages inside a reasonable range.

C. Containment and Consensus-based Controller in the Secondary Control Level

The containment-based voltage controller generates a correction item e_{Vi} for each DG to bound all bus voltages within a reasonable range. The range in the algorithm is formed by upper bound V_{Ubou} and lower bound V_{Lbou}. The controller is defined as

$$\dot{e}_{Vi} = -\sum_{j \in N_i} a_{ij} \left(V_{ci} - V_{cj} \right) - \sum_{l \in R_i} b_{il} \left(V_{ci} - V_{bou} \right) \qquad (2)$$

where V_{bou} is the voltage boundary reference which can be either upper boundary V_{Ubou} or lower boundary V_{Lbou}.

Eq. (2) can be written into matrix formation as

$$\dot{e}_V = -L_V V_C - L_{Bou} V_{Bou} \qquad (3)$$

where $e_V = \begin{bmatrix} e_{V1} & \cdots & e_{Vn} \end{bmatrix}^T$, $V_C = \begin{bmatrix} V_{c1} & \cdots & V_{cn} \end{bmatrix}^T$,
$V_{Bou} = \begin{bmatrix} V_{Ubou} & V_{Lbou} \end{bmatrix}^T$.

Then $\dot{e}_{Vi}$ is fed into a *PI* controller defined as: $G_{Vi} = k_{pVi} + k_{iVi}/s$ in which s is the laplace operator. Then the compensating item from containment-based voltage controller for i_{th} DG can be written as:

$$V_{comi} = k_{pVi}\dot{e}_{Vi} + k_{iVi}e_{Vi} \qquad (4)$$

The consensus-based current controller generates correction item e_{RIi} to achieve precise current sharing between DGs, which can be written as:

$$\dot{e}_{RIi} = -\sum_{j \in N_i} a_{ij}\left(R_{viri}I_{oi} - R_{virj}I_{oj}\right) \qquad (5)$$

where I_{oi} is the filter output current from i_{th} DG.

Eq. (5) can be rewritten into matrix formation as

$$\dot{e}_{RI} = -L_I R_{vir} I_O \qquad (6)$$

where $e_{RI} = \begin{bmatrix} e_{RI1} & \cdots & e_{RIn} \end{bmatrix}^T$, $R_{vir} = diag\left\{ \begin{bmatrix} R_{vir1}, & \cdots & R_{virn} \end{bmatrix}^T \right\}$,
$I_O = \begin{bmatrix} I_{o1} & \cdots & I_{on} \end{bmatrix}^T$.

Then $\dot{e}_{RIi}$ is fed into another *PI* controller: $G_{Ii} = k_{pIi} + k_{iIi}/s$. The compensating item from consensus-based current controller for i_{th} DG is written as

$$I_{comi} = \frac{1}{R_{viri}}\left(k_{pIi}\dot{e}_{RIi} + k_{iIi}e_{RIi}\right) \qquad (7)$$

By adding the proposed voltage and current controller given in eq. (4) and (7), eq. (1) can be changed as

$$I_{refi} = \frac{V_{ref} - V_{ci} + V_{comi}}{R_{viri}} + I_{comi} \qquad (8)$$

The configuration of proposed controller discussed above is shown in Fig. 1 including the reverse droop controller, the containment-based voltage controller and the consensus-based current controller. For the communication structure in the system, the information format from DGs (followers) is defined as $\Upsilon_{fj} = \begin{bmatrix} R_{virj}I_{oj}, & V_j \end{bmatrix}$, the information format from the leader is defined as $\Upsilon_l = \begin{bmatrix} 0, & V_{bou} \end{bmatrix}$.

III. LARGE SIGNAL MODEL AND STABILITY ANALYSIS

This section develops the large signal model for stability analysis. The model includes proposed containment-based voltage controller and consensus-based current power controller, reverse droop control, inner current control loop, electrical model for a dc MG.

A. Large Signal Model for the Whole System
Substituting eq. (4) and (7) in eq. (8), it can be rewritten as

$$I_{refi} = \frac{V_{ref} - V_{ci} + \overbrace{k_{pVi}\dot{e}_{Vi} + k_{iVi}e_{Vi}}^{V_{comi}}}{R_{viri}} + \overbrace{\frac{1}{R_{viri}}\left(k_{pIi}\dot{e}_{RIi} + k_{iIi}e_{RIi}\right)}^{I_{comi}} \qquad (9)$$

Substituting eq. (3) and (6) in eq. (9), it can be rewritten as (matrix formation)

$$I_{Ref} = R_{vir}^{-1}\begin{bmatrix} V_{Ref} - V_C + K_{pV}\left(-L_V V_C - L_{Bou}V_{Bou}\right) \\ +K_{iV}e_V + K_{pI}\left(-L_I R_{vir}I_O\right) + K_{iI}e_{RI} \end{bmatrix} \qquad (10)$$

where $K_{pV} = diag\left(\begin{bmatrix} k_{pV1} & \cdots & k_{pVn} \end{bmatrix}^T \right)$, $K_{iV} = diag\left(\begin{bmatrix} k_{iV1} & \cdots & k_{iVn} \end{bmatrix}^T \right)$, $K_{iI} = diag\left(\begin{bmatrix} k_{iI1} & \cdots & k_{iIn} \end{bmatrix}^T \right)$, $K_{pI} = diag\left(\begin{bmatrix} k_{pI1} & \cdots & k_{pIn} \end{bmatrix}^T \right)$, $I_{Ref} = \begin{bmatrix} I_{ref1} & \cdots & I_{refn} \end{bmatrix}^T$, $R_{vir} = diag\left(\begin{bmatrix} R_{vir1} & \cdots & R_{virn} \end{bmatrix}^T \right)$, $V_{Ref} = 1_n V_{ref}$.

To make eq. (10) more clear, it can be rewritten as

$$\begin{aligned} I_{Ref} &= R_{vir}^{-1}\left(-I_n - K_{pV}L_V\right)V_C - R_{vir}^{-1}K_{pI}L_I R_{vir}I_O \\ &\quad + R_{vir}^{-1}K_{iV}e_V + R_{vir}^{-1}K_{iI}e_{RI} + R_{vir}^{-1}V_{Ref} \\ &\quad - R_{vir}^{-1}K_{pV}L_{Bou}V_{Bou} \end{aligned} \qquad (11)$$

Since the dynamic response of inner current loop is much faster than that of the outer control loop, the inner current loop *PI* controller and the inductor of the *LC* filter with its equivalent resistance can be approximated as a first-order lag

$$G_C(s) = 1/(\tau s + 1) \qquad (12)$$

where $1/\tau$ is the equivalent control bandwidth.

Thus, the relationship between I_{refi} and I_{oi} can be written as

$$I_{oi} = \frac{1}{\tau s + 1}I_{refi} \xrightarrow{\text{Matrix Formation}} \dot{I}_O = \Gamma\left(I_{Ref} - I_O\right) \qquad (13)$$

where $\Gamma = 1/\tau I_n$.

Substituting eq. (11) into eq. (13), it can be rewritten as

$$\begin{aligned} \dot{I}_O &= \Gamma R_{vir}^{-1}\left(-I_n - K_{pV}L_V\right)V_C \\ &\quad + \Gamma\left(-R_{vir}^{-1}K_{pI}L_I R_{vir} - I_n\right)I_O + \Gamma R_{vir}^{-1}K_{iV}e_V \\ &\quad + \Gamma R_{vir}^{-1}K_{iI}e_{RI} + \Gamma R_{vir}^{-1}V_{Ref} - \Gamma R_{vir}^{-1}K_{pV}L_{Bou}V_{Bou} \end{aligned} \qquad (14)$$

Furthermore, the voltage boundary can be acquired through multiplying the nominal voltage V_{ref} and standard percentage *Per*. The relationship between the V_{ref} and V_{Ubou}, V_{Lbou} is written as

$$\begin{cases} V_{Ubou} = (1 + Per)V_{ref} \\ V_{Lbou} = (1 - Per)V_{ref} \end{cases} \Rightarrow \begin{bmatrix} V_{Ubou} \\ V_{Lbou} \end{bmatrix} = PV_{ref} \qquad (15)$$

where $P = \begin{bmatrix} 1 + Per & 1 - Per \end{bmatrix}^T$.

Thus, eq. (14) can be rewritten as

$$\begin{aligned} \dot{I}_o &= \Gamma R_{vir}^{-1}\left(-I_n - K_{pV}L_V\right)V_C \\ &\quad + \Gamma\left(-R_{vir}^{-1}K_{pI}L_I R_{vir} - I_n\right)I_O + \Gamma R_{vir}^{-1}K_{iV}e_V \\ &\quad + \Gamma R_{vir}^{-1}K_{iI}e_{RI} + \left(\Gamma R_{vir}^{-1} - \Gamma R_{vir}^{-1}K_{pV}L_{Bou}P\right)V_{Ref} \end{aligned} \qquad (16)$$

Furthermore, due to the effects from output capacitors, the relationship among output voltage V_{ci}, filter current I_{oi} and current I_{ti} for loads and line impedances can be modelled as

$$V_{ci} = \frac{1}{sC}\left(I_{oi} - I_{ti}\right) \xrightarrow{\text{Matrix Formation}} \dot{V}_C = Cap^{-1}\left(I_O - I_T\right) \quad (17)$$

where C is the value for output capacitors (for all the converters, the capacitor value is same), $Cap = C * I_n$.

Based on the relationship between current I_T and bus voltage V_C which is established in [13], eq. (17) can be rewritten as

$$\dot{V}_C = Cap^{-1}\left(I_O - L_T V_C\right) \quad (18)$$

where L_T is the bus admittance matrix.

Combing with eq. (3), (6), (16) and (18), the whole system model can be written as

$$
\begin{bmatrix} \dot{V}_C \\ \dot{I}_O \\ \dot{e}_V \\ \dot{e}_{RI} \end{bmatrix} = \underbrace{\begin{bmatrix} -Cap^{-1}L_T & Cap^{-1} & 0_{[n]} & 0_{[n]} \\ \Gamma R_{vir}^{-1}\left(-I_n - K_{pV}L_V\right) & \Gamma\left(-R_{vir}^{-1}K_{pI}L_I R_{vir} - I_n\right) & \Gamma R_{vir}^{-1}K_{iV} & \Gamma R_{vir}^{-1}K_{iI} \\ -L_V & 0_{[n]} & 0_{[n]} & 0_{[n]} \\ 0_{[n]} & -L_I R_{vir} & 0_{[n]} & 0_{[n]} \end{bmatrix}}_{A} \begin{bmatrix} V_C \\ I_O \\ e_V \\ e_{RI} \end{bmatrix}
$$

$$
+ \underbrace{\begin{bmatrix} 0_n \\ \left(\Gamma R_{vir}^{-1} - \Gamma R_{vir}^{-1}K_{pV}L_{Bou}P\right) \\ -L_{Bou}P \\ 0_n \end{bmatrix}}_{B} V_{ref}
$$

$$(19)$$

B. Stability Analysis

To analyze the sensitivity of coefficients in the proposed controllers quantitatively, a dc MG including four parallel connected DGs, line impedances, loads are considered as a study case. The system parameters are given in Table I. Pole-zero locus by changing different control coefficients are shown in Fig. 2-5 to analyze the dynamic behavior of the system.

Fig. 2 shows the pole-zero locus with the proportional coefficient K_{pV} changed from 0.1 to 5 in PI controller for containment-based control loop. A pair of dominating poles is moving away from the real axis indicating that the system is becoming less damped. The zoom in part of Fig. 2 shows that the poles are moving towards the real axis meaning that the system is becoming less damped and the response speed is becoming slower. Other pairs of poles also indicate that the system is becoming less damped. Fig. 3 shows pole-zero locus with integral coefficient K_{iV} changed from 1 to 300 for containment-based control loop. The zoom in part of Fig. 3 shows that one dominating pole on the real axis is moving away from the imaginary axis and a pair of poles is moving toward the imaginary axis, which means that the response speed of the system is enhanced. Three poles on the real axis is moving away from the imaginary axis which can increase the dynamic response speed. Another three pairs of poles moving toward the real axis can make the system more damped.
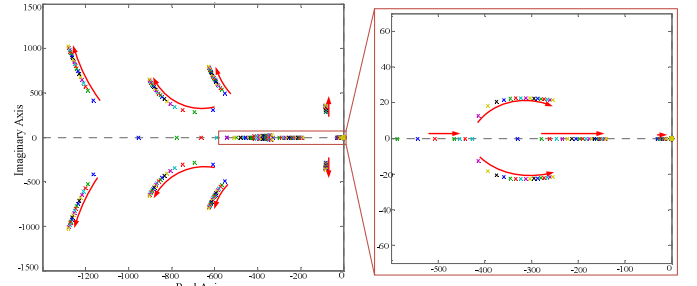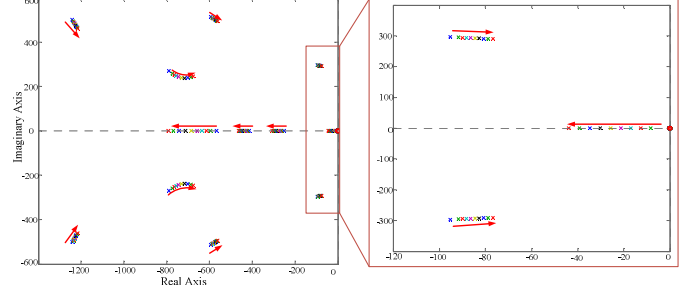

Fig. 2. Root locus plot $0.1 < K_{pV} < 5$.

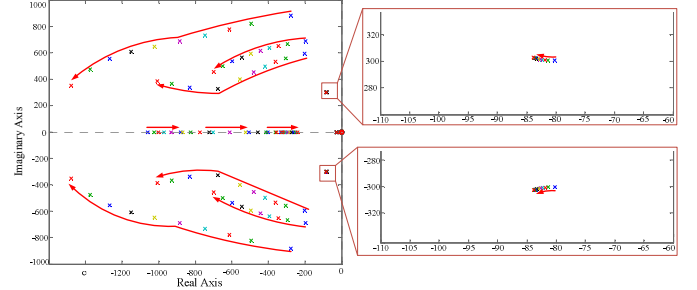Fig. 3. Root locus plot $1 < K_{iV} < 300$.
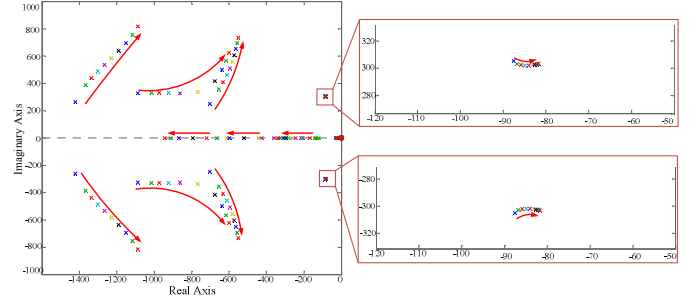

Fig. 4. Root locus $0.1 < K_{pI} < 1$.

Fig. 5. Root locus plot $1 < K_{iI} < 600$.

Fig. 4 shows pole-zero locus with proportional coefficients K_{pI} in PI controller for consensus-based current control changed from 0.1 to 1. From the zoom in part, it shows that a pair of dominating poles is moving away from the original point making system more damped and transient response speed more quickly. Meanwhile, three pairs of poles are moving away from the imaginary axis and towards the real axis which indicate that the response speed is enhanced and the system is becoming more damped. Fig. 5 shows pole-zero locus considering integral coefficients K_{iI} changed from 1 to 600 in PI controller for consensus-based current control. From the zoom in part, it shows that a pair of dominating poles is moving towards the imaginary axis which means the system is becoming less damped. Except for that, three pairs of poles are

moving away from the real axis also meaning that the system is becoming less damped.

Based on above analysis, the control coefficients are chosen, which are shown in Table I.

IV. EXPERIMENTAL RESULTS

The proposed control scheme is implemented and tested in an experimental dc MG setup operated in islanded mode shown in Fig. 6. The setup consists of four parallel-configured dc-dc buck converters, LC filters, different line impedances, loads, dSPACE controller and monitoring platform. Communication link is shown in the top left corner of Fig. 6 which is a distributed communication structure. The ratio for four converters' rated capacity is 2: 2: 1: 1 from converter 1 to 4. The nominal voltage for the dc MG is 120 V. According to the standard [14], the upper voltage boundary is set as *122V* which is smaller than *120*(1+2%)V*, while the lower voltage boundary is set as *118V* which is larger than *120*(1-2%)V*. The experimental results are shown in Fig. 7-9.

TABLE I
Experimental Setup and Control Coefficients

|	Coefficients	Value
Electrical Setup Parameters	Filter Inductor	1.8 *mH*
	DC Bus Capacitance	2200 *uF*
	Line impedance for Converter 1	0.7 *Ω*+1.2 *mH*
	Line impedance for Converter 2	1.3 *Ω*+1.5 *mH*
	Line impedance for Converter 3	0.4 *Ω*+1.2 *mH*
	Line impedance for Converter 4	1.6 *Ω*+1.7 *mH*
Inner Current Loop Controller	Current proportional coefficient	0.003
	Current integral coefficient	0.1
Droop Controller	Droop Coefficients for Converter 1 and 2 (R_{vir1} and R_{vir2})	0.6
	Droop Coefficients for Converter 3 and 4 (R_{vir3} and R_{vir4})	1.2
Containment-based Voltage Controller	Proportional coefficient for communication matrix L_V	0.2
	Proportional coefficient (K_{pVi})	0.5
	Integral coefficient (K_{pIi})	90
Consensus-based Current Controller	Proportional coefficient for Communication matrix L_I	2.5
	Proportional coefficient (K_{pIi})	0.8
	Integral coefficient (K_{iIi})	400
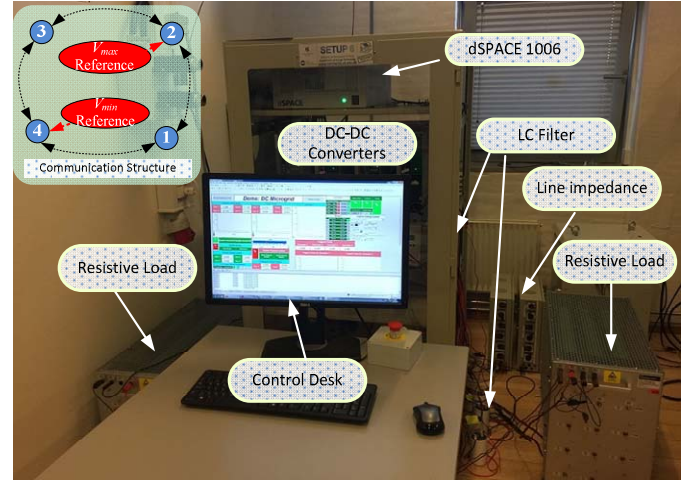
Fig. 6. Experimental setup in AAU-Microgrid research laboratory

A. Case 1: Control Performance Test with Proposed Control Strategy

Fig. 7 shows the control performance by combining the proposed controller with reverse droop control. At t=*T1*, the proposed controller is activated. Before t=*T1*, the output current cannot be shared accurately due to the different line impedances effects and voltage deviations from nominal value exist by using reverse droop control. After activating the proposed controller, it is shown in Fig. 7 (a) that the output voltages can be bounded within the boundary while keeping the necessary deviations between each other around nominal value to guarantee the power flow achieving accurate current sharing. In addition, the per unit current values shown in Fig. 7 (b) proves that the proposed controller can achieve proportional current sharing accurately. At the t=*T1* and *T3*, the load is increased and decreased respectively, both the two control objectives are guaranteed.

(a). Performance of Output Voltage
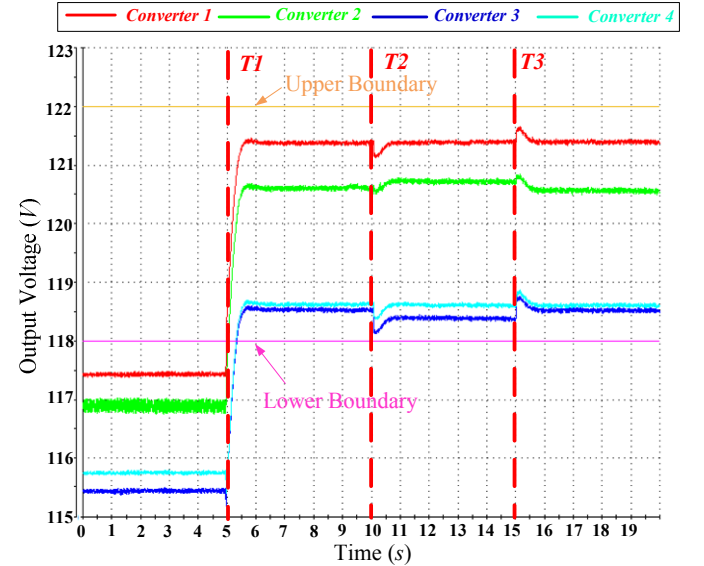
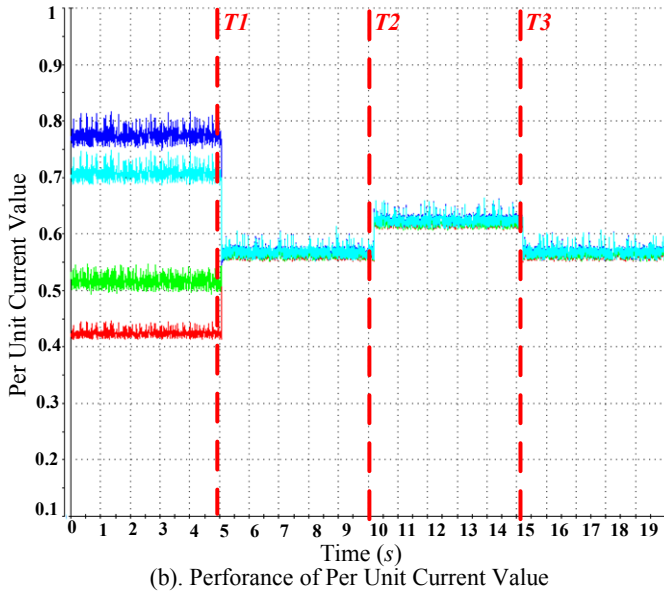(b). Perforance of Per Unit Current Value

Fig. 7 Control Performance Comparison for Case 1: (a) Output Voltage; (b) Per Unit Output Current.

B. Case 2: Control performance under dynamic voltage boundary;

Fig. 8 shows performance of the proposed controller with dynamic voltage boundary. At t=*T1*, the proposed controller is activated. Between t=*T2* and *T5*, the voltage boundary is changed. As shown in Fig. 8 (a), the output voltages can follow the dynamic voltage boundary very well, while the accurate current sharing is achieved simultaneously as shown in Fig. 8 (b). During the period between *T2* and *T5*, the load is increased and decreased at t=*T3* and *T4* respectively; The accurate current sharing can also be guaranteed as shown in Fig. 8 (b). At t=*T5*, when the voltage boundary is set back to the nominal range, the performance of voltage bound and accurate current sharing can also be guaranteed.
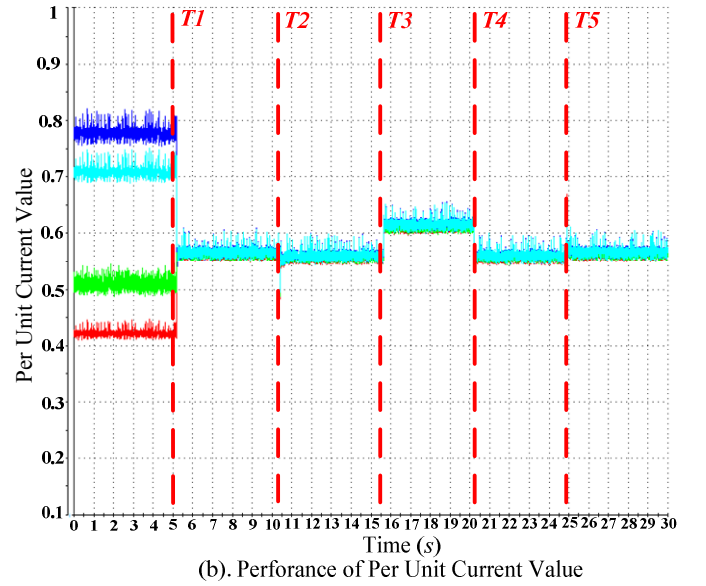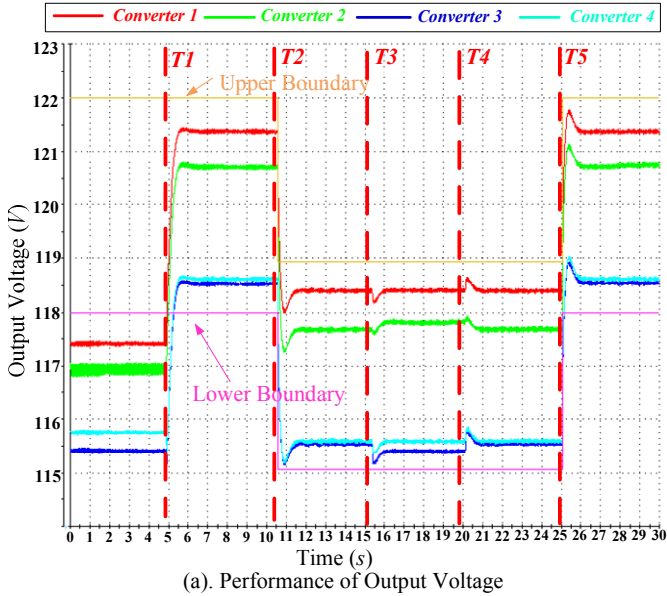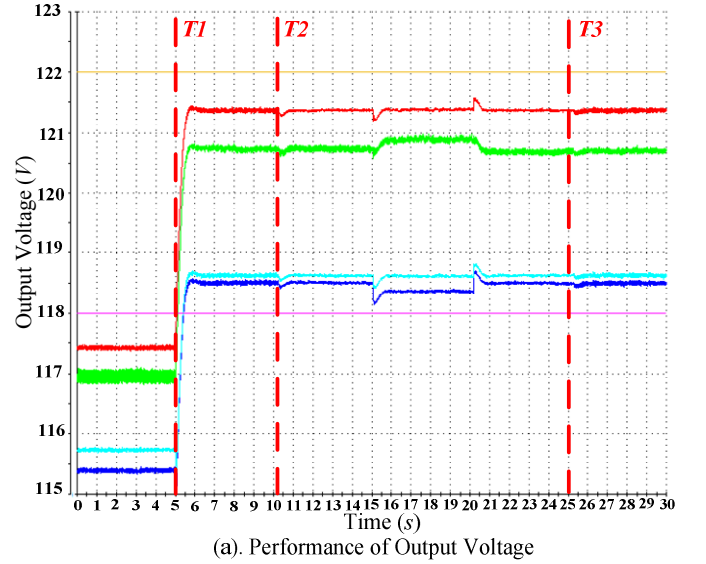

(a). Performance of Output Voltage

(b). Perforance of Per Unit Current Value

Fig. 8. Control Performance for Case 2: (a) Output Voltage; (b) Per Unit Output Current.

C. Case 3: Control performance under Communication Failure

Fig. 9 shows performance of the proposed controller under communication failure condition. At t=*T1*, the proposed controller is activated. Between t=*T2* and *T3*, the communication link between converter 2 and converter 3 is disabled. It is shown in Fig. 9 (a), when communication is disenabled, small oscillations exist in the transient response of output voltages. When the load is increased and decreased respectively during the communication failure period, both the bounded bus voltage and accurate current sharing can also be guaranteed shown in Fig. 9 (a) and (b), the communication failure cannot affect the steady-state control performance.
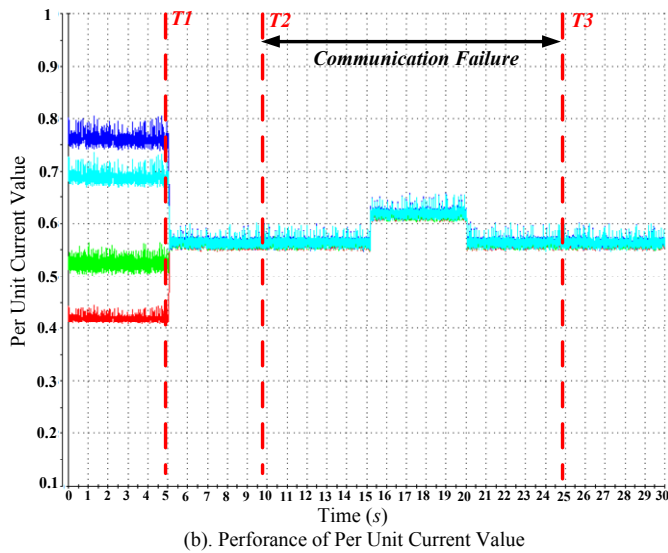

(a). Performance of Output Voltage

(b). Perforance of Per Unit Current Value

Fig. 9. Control Performance for Case 3: (a) Output Voltage; (b) Per Unit Output Current.

V. CONCLUSION

A distributed coordination control including both containment and consensus-based controllers is proposed to offer a highly flexible and reliable operation for reverse droop based dc MG, achieving dynamic bounded bus voltage and accurate current power sharing regulation. The proposed algorithm cannot only guarantee the power quality for public load but also for local load due to the bounded bus voltages. Combining the proposed controller with the electrical topology of dc MG, the model is derived, based on which the pole-zero locus are conducted to analyze the influence of different control coefficients for the whole system. Experimental results including the comparison test, dynamic voltage boundary change test and communication resiliency test are presented to demonstrate the effectiveness of proposed controllers.

REFERENCES

[1] A. Ipakehi, F. Albuyeh, "Grid of the future," *Power and Energy Magazine, IEEE*, vol. 7, no. 2, pp. 52-62, 2009.

[2] N. Hatziargyriou, H, Asano, R. Iravani, and C. Marnay, "Microgrids," *Power and Energy Magazine, IEEE,* vol. 5, no. 4, pp. 78-94, Jul. 2007.

[3] L. Meng, T. Dragicevic, J. Roldan-Perez, J. C. Vasquez, J. M. Guerrero, "Modeling and sensitivity study of consensus algorithm-based distributed hierarchical control for DC microgrid," *IEEE Trans. Smart Grid*, vol. 7, no. 3, pp. 1504-1515, May 2016.

[4] F. Gao, S. Bozhko, A. Costabeber, C. Patel, P. Wheeler, C. Hill, G. Asher, "Comparative stability analysis of droop control approaches in voltage source converters-based dc microgrid," *IEEE Trans. Power Electron.*, vol. 32, no. 3, pp. 2395-2415, May. 2017

[5] X. Lu, K. Sun, J. M. Guerrero, J. C. Vasquez, and L. Huang, "State-of-charge balance using adaptive droop control for distributed energy storage system in DC microgrid applications," *IEEE Trans. Ind. Electron.*, vol. 61, no. 6, pp. 2804-2815, Jun. 2014.

[6] J. M. Guerrero, J. C. Vasquez, J. Matas, M. Castilla, L. G. D. Vicuna, and M. Castilla, "Hierarchical control of droop-controlled ac and dc microgrids—A general approach toward standardization," *IEEE Trans. Ind. Electron.*, vol. 58, no. 1, pp. 158-172, Jan. 2011.

[7] S. Anand, B. G. Fernandes, and J. M. Guerrero, "Distributed control to ensure proportional load sharing and improve voltage regulation in low-voltage DC microgrids," *IEEE Trans. Power Electron.*, vol. 28, no. 4, pp. 1900-1913, Apr. 2013.

[8] X. Lu, J. M. Guerrero, K. Sun, and J. C. Vasquez, "An improved droop control method for dc microgrids based on low bandwidth communication with dc bus voltage restoration and enhanced current sharing accuracy," *IEEE Trans. Power Electron.*, vol. 29, no. 4, pp. 1800-1812, Apr. 2014.

[9] V. Nasirian, A. Davoudi, F. L. Lewis, J. M. Guerrero, "Distributed adaptive droop control for DC distribution system," *IEEE Trans. Energy Convers.*, vol. 29, no. 4, pp. 944-956, Feb. 2014.

[10] R. Olfati-Saber, J. A. Fax, and R. M. Murray, "Consensus and cooperation in networked multi-agent systems," *Proc. IEEE*, vol. 95, no. 1. Pp. 215-233, Jan. 2007.

[11] V. Nasirian, S. Moayedi, A. Davoudi, and F. L. Lewis, "Distributed cooperative control of DC microgrids," *IEEE Trans. Power Electron.*, vol. 30, no. 4, pp. 2288-2303, Apr. 2015.

[12] C. Gavriluta, I. Candela, A. Luna, A. G. Exposito, P. Rodriguez, "Hierarchical control of HV-MTDC systems with droop-based primary and OPF-based secondary," *IEEE Trans. Smart Grid*, vol. 6, no. 3, pp. 1502-1510, May, 2015.

[13] R. Han, N. L. Aldana, L. Meng, J. M. Guerrero, Q. Sun, "Droop-free distributed control with event-triggered communication in DC micro-grid," *IEEE Applied Power Electronics Conference (APEC)*, 2017.

[14] R. A. F. Ferreira, H. A. C. Braga, A. A. Ferreira, and P. G. Barbosa, "Analysis of voltage droop control method for DC microgrids with simulink: Modeling and simulation," in Proc. 10th IEEE/IAS Int. Conf. Ind. Appl., 2012, pp. 1–6.